Journal of Geophysical Research: Space Physics

RESEARCH ARTICLE
10.1029/2017JA024618

One-Hertz Waves at Mars: MAVEN Observations

Suranga Ruhunusiri[1], J. S. Halekas[1], J. R. Espley[2], F. Eparvier[3], D. Brain[3], C. Mazelle[4], Y. Harada[1], G. A. DiBraccio[2], E. M. B. Thiemann[3], D. E. Larson[5], D. L. Mitchell[5], B. M. Jakosky[3], and A. H. Sulaiman[1]

[1]Department of Physics and Astronomy, The University of Iowa, Iowa City, IA, USA, [2]NASA Goddard Space Flight Center, Greenbelt, MD, USA, [3]Laboratory for Atmospheric and Space Physics, University of Colorado Boulder, Boulder, CO, USA, [4]IRAP, University of Toulouse, CNRS, UPS, CNES, Toulouse, France, [5]Space Sciences Laboratory, University of California, Berkeley, CA, USA

Abstract We perform a survey of 1-Hz waves at Mars utilizing Mars Atmosphere and Volatile EvolutioN (MAVEN) spacecraft observations for a Martian year. We find that the 1-Hz wave occurrence rate shows an apparent variation caused by masking of the waves by background turbulence during the times when the background turbulence levels are high. To correct for this turbulence masking, we select waves that occur in time intervals where the background turbulence levels are low. We find that the extreme ultraviolet flux does not affect the wave occurrence rate significantly, suggesting that the newly born pickup ions originating in the Mars's exosphere contribute minimally to the 1-Hz wave generation. We find that the wave occurrence rates are higher for low Mach numbers and low beta values than for high Mach numbers and high beta values. Further, we find that a high percentage of 1-Hz waves satisfy the group-standing condition, which suggests that a high percentage of the waves seen as monochromatic waves in the spacecraft frame can be broadband waves in the solar wind frame that have group velocities nearly equal and opposite to the solar wind velocity. We infer that the wave occurrence rate trends with the Mach number and proton beta are a consequence of how the Mach numbers and beta values influence the wave generation and damping or how those parameters affect the group-standing condition. Finally, we find that the 1-Hz waves are equally likely to be found in both the quasi-parallel and the quasi-perpendicular foreshock regions.

Key Points:
- One-hertz waves at Mars show an apparent occurrence rate variation due to masking of the waves during times of high background turbulence levels
- The wave occurrence rates vary significantly with Mach numbers and proton beta values but do not vary significantly with EUV flux levels
- The 1-Hz waves are observed in both the quasi-parallel and quasi-perpendicular foreshock regions with comparable occurrence rates

Correspondence to:
S. Ruhunusiri,
suranga-ruhunusiri@uiowa.edu

Citation:
Ruhunusiri, S., Halekas, J. S., Espley, J. R., Eparvier, F., Brain, D., Mazelle, C., et al. (2018). One-hertz waves at Mars: MAVEN observations. *Journal of Geophysical Research: Space Physics*, *123*. https://doi.org/10.1029/2017JA024618

Received 21 JUL 2017
Accepted 31 MAR 2018
Accepted article online 9 APR 2018

1. Introduction

One-hertz waves are whistler mode waves, which have frequencies near 1 Hz as measured in a spacecraft frame, and these waves are observed frequently in planetary upstream regions. These low-frequency upstream whistler waves have been observed at Mercury (Fairfield & Behannon, 1976; Le et al., 2013; Orlowski et al., 1990, 1995; Russell, 2007), Venus (Orlowski et al., 1990; Orlowski & Russell, 1991; Orlowski et al., 1995; Russell, 2007), Earth (Balikhin et al., 1997; Fairfield, 1974; Greenstadt et al., 1995; Heppner et al., 1967; Holzer et al., 1972; Hoppe et al., 1981, 1982; Orlowski et al., 1990, 1995; Russell et al., 1971; Russell & Farris, 1995; Russell, 2007; Tsurutani et al., 2001), Mars (Brain et al., 2002), Saturn (Orlowski et al., 1992, 1995; Russell, 2007; Sulaiman et al., 2017), Jupiter (Tsurutani et al., 1993), Uranus (Smith et al., 1989, 1991), the Moon (Halekas et al., 2006, 2013; Nakagawa et al., 2003, 2011; Tsugawa et al., 2011, 2012, 2014, 2015), and at interplanetary shocks (Ramírez Vélez et al., 2012; Wilson et al., 2009). The frequency of these waves monotonically decreases for planets that are farther away from the Sun. For example, at Mercury, these waves typically have frequencies close to 2 Hz, whereas at Saturn, these waves have frequencies close to 0.1 Hz (Orlowski et al., 1990). However, the frequencies of these waves, as observed in the spacecraft frame, are typically higher than the local proton gyrofrequency. Upstream whistlers are observed as circularly or elliptically polarized waves. While these waves are intrinsically right-hand polarized, they are observed in both right-hand and left-hand polarization states in a spacecraft frame. This is a consequence of Doppler shift, where the intrinsically right-hand polarized waves that propagate toward the Sun at small angles are swept back by the solar wind flow undergoing maximal Doppler shift and are seen as left-hand polarized waves, whereas the waves that propagate at larger angles suffer minimal Doppler shift and are seen in their intrinsic right-hand polarized state (Fairfield, 1974; Orlowski & Russell, 1991). The amplitude of these waves gradually decreases with increasing distance from the bow shock indicating that the waves are generated at the bow shock or upstream of the bow shock. These

waves can also be seen far upstream of the bow shock as their group velocities can exceed the solar wind flow velocity enabling them to propagate upstream against the solar wind flow.

While there are numerous observations of 1-Hz whistler waves throughout the solar system, their exact generation mechanism remains elusive. A variety of mechanisms has been proposed as the sources of these waves. These include, upstream ion beams (Gurgiolo et al., 1993; Hellinger & Mangeney, 1997; Hellinger et al., 1996; Hoppe et al., 1981, 1982; Krauss-Varban et al., 1995; Wong & Goldstein, 1987, 1988), electron beams (Feldman et al., 1983; Sentman et al., 1983; Smith et al., 1991; Wong & Smith, 1994), steepening of low-frequency waves (Bertucci et al., 2007; Hoppe & Russell, 1980; Tsurutani et al., 1993), generation at the bow shock through processes such as cross field and anisotropy-driven instabilities (Orlowski et al., 1995), and nonlinear phenomena associated with the bow shock (Balikhin et al., 1997; Hellinger et al., 2007; Krasnoselskikh et al., 2002; Walker et al., 1999).

At Mars, Brain et al. (2002) made the first observation and characterization of 1-Hz whistler waves utilizing Mars Global Surveyor measurements spanning a time period from 13 September 1997 to 23 September 1998. These waves were observed upstream of the planetary bow shock and these waves had frequencies between 0.4 Hz and 2.3 Hz. The waves were mostly transverse; that is, the waves had more power transverse to the magnetic field than parallel to it. The waves were also elliptically polarized, and they propagated at oblique angles to the ambient magnetic field. In particular, the angles between the magnetic field and the wave vector θ_{kB} were typically between 19° and 40°. Waves that propagated at smaller angles to the sunward direction, that is, below 66°, were found to be left-hand polarized, whereas waves that propagated at higher sunward angles were found to be right-hand polarized. This trend in the wave polarization with the sunward angles was explained by Brain et al. (2002) in terms of Doppler shift. In this study Brain et al. (2002) were able to observe 1-Hz waves at Mars to a distance of 10 planetary radii. However, the wave amplitudes were found to diminish with increasing distance from the planetary bow shock. Brain et al. (2002) suggested that these waves are generated in the upstream region of Mars due to bow shock and foreshock phenomena in analogy with other planets. Recently, 1-Hz waves at Mars have also been observed by the Mars Atmosphere and Volatile EvolutioN (MAVEN) spacecraft (Connerney et al., 2015).

In this study, we use the MAVEN spacecraft observations to characterize 1-Hz waves using observations spanning a single Martian year. MAVEN's science orbit has a period of 4.5 hr with an apoapsis of 6,200 km and a periapsis of 150 km. Its orbit precesses in such a way that the apoapsis is located in the undisturbed solar wind upstream from the bow shock at times and inside the induced magnetosphere at other times (Jakosky et al., 2015). When the spacecraft apoapsis is located upstream of the bow shock, upstream measurements can be obtained for typically 4 to 5 months. In between this 4- to 5-month time segments we lose the upstream coverage for typically 2 months because of the precession of the spacecraft apoapsis to the night side. Thus, MAVEN's orbit enables obtaining a large number of measurements in the upstream region and this is ideal for studying upstream phenomena at Mars. For the study of 1-Hz waves, we have the following objectives: (1) Determine how the upstream drivers such as extreme ultraviolet (EUV) flux, Mach number, and plasma beta influence the wave occurrence rate. (2) Determine how the wave occurrence rate varies in the quasi-parallel and quasi-perpendicular foreshock regions.

The EUV flux levels vary at Mars due to changes in the Mars-Sun distance as Mars revolves around the Sun. Mars's hydrogen exospheric density increases with the increasing EUV flux levels (Halekas et al., 2017; Yamauchi et al., 2015) and that the upstream waves, such as proton cyclotron waves, can be excited by resonance with newly born pickup protons (Bertucci et al., 2005; Delva et al., 2011; Mazelle et al., 2004; Romanelli et al., 2013; Ruhunusiri et al., 2016; Russell et al., 1990). Thus, if the 1-Hz waves are generated by resonance with newly born pickup protons originating in Mars's extended exosphere, we would expect the wave occurrence rate to increase with the increasing EUV flux levels. However, EUV is not always the dominant source for pickup ions (Curry, Liemohn, Fang, Brain, et al., 2013; Curry, Liemohn, Fang, Ma, et al., 2013). Similarly, if the 1-Hz waves are generated by steepening of low-frequency waves such as the proton cyclotron waves, we would also expect the 1-Hz wave occurrence rate to be high during the times of high EUV flux levels where the proton cyclotron waves have been observed to have a high occurrence rate (Romanelli et al., 2016; Ruhunusiri et al., 2017). Barabash and Lundin (1993) and Yamauchi et al. (2011) observed upstream ion populations at Mars, using Phobos 2 and Mars Express observations, which were suggested as reflected ions from the bow shock. Recently, Meziane et al. (2017) observed electron populations upstream of Mars's bow shock using MAVEN observations, which were interpreted as reflected solar wind electrons from the bow shock.

Thus, it is conceivable that such reflected particles can generate 1-Hz waves. If the 1-Hz waves are generated due to resonance with reflected ions from the bow shock, we would expect to observe a high wave occurrence rate at high Mach number conditions as these conditions lead to a greater proportion of reflected particles from the bow shock (Leroy et al., 1982). If the 1-Hz waves are preferentially observed in the quasi-parallel foreshock region, it is indicative of generation of waves via resonance with field-aligned beams. High electron beta conditions lead to increased wave damping via Landau damping (Gary & Mellott, 1985). Thus, we would expect to see a lower occurrence rate of 1-Hz waves for high electron beta conditions if Landau damping is effective at damping these waves. Thus, determining whether the 1-Hz wave occurrence rates show any variations with the upstream parameters and variations in quasi-parallel and quasi-perpendicular foreshock regions may enable us to identify how the waves are generated and damped.

2. Method

To identify 1-Hz waves, we use a method that is similar to the ones that were employed by Brain et al. (2002) and Halekas et al. (2006) in their studies of 1-Hz waves at Mars and the Moon. In particular, we identify 1-Hz waves using an automated search procedure. We start with a time series of the full resolution (32 Hz) vector magnetic field in the Mars Solar Orbital coordinate system (see Figure 1b), which is measured by the MAVEN magnetometer (Connerney, Espley, DiBraccio et al., 2015; Connerney, Espley, Lawton, et al., 2015). Then using a 32-s window, we take the Fourier transform of each component of the magnetic field using a Hanning window every 32 s and compute the magnetic field power spectra (shown in Figure 1c). We search for peaks in the power spectra for frequencies between $3f_i$ and 3 Hz, where f_i is the local proton gyrofrequency (see Figure 3b of Ruhunusiri et al., 2017, for a distribution of f_i in the Mars plasma environment). Here the lower-frequency limit of $3f_i$ was selected to avoid selection of proton cyclotron waves, and 3 Hz was used as the upper-frequency limit because Brain et al. (2002) did not find any low-frequency upstream whistler waves above 3 Hz. To identify peaks, first, we select the frequency where the power attains a maximum value. Then we require that the power at that frequency be at least 3 times higher than the mean power in the low-frequency range spanning $3f_i$ to $f - 2\delta_f$ and be at least 4 times higher than the mean power in the high-frequency range $f + 2\delta_f$ to 3 Hz, where f is the frequency corresponding to the maximum power and δ_f is the frequency resolution of the fast Fourier transform power spectra. Here we select a lower power threshold for the low-frequency range, since the turbulence levels in the low-frequency range are higher than the high-frequency range (Ruhunusiri et al., 2017). We find that this selection of a factor of 3 and 4 in the low- and high-frequency ranges, respectively, for the peak identification ensures that the 1-Hz waves that can be discerned by a visual survey of the power spectra are identified in the automated search routine as 1-Hz waves (see Figures 1c and 1d). We also require that the power of a peak be greater than 0.5 nT^2/Hz to ensure that the spacecraft reaction wheel signatures are not misidentified as 1-Hz waves. These reaction wheel signatures can be seen for frequencies below 3 Hz occasionally, and the power of these signatures is typically 0.1 nT^2/Hz or lower. Using the method described above, we identify 1-Hz waves for the following time periods where MAVEN had upstream coverage: 1 December 2014 to 17 March 2015, 4 June 2015 to 25 October 2015, 5 December 2015 to 12 April 2016, 1 June 2016 to 30 September 2016, and 1 December 2016 to 31 March 2017.

We plot the distributions of the EUV flux, the magnetosonic Mach number, and proton beta in Figure 2 for all the time periods mentioned above, and we use these distributions to determine how the wave occurrence rate varies with these parameters as will be described in section 3. MAVEN's Extreme Ultraviolet Monitor measurements (Eparvier et al., 2015) are used to determine the EUV flux (Lyman-alpha flux) shown in Figure 2a. We compute the upstream magnetosonic Mach number and proton beta (shown in Figures 2b and 2c) using MAVEN's Solar Wind Ion Analyzer (SWIA) measurements of the ion moments and the magnetometer measurements of the magnetic field as described in p. 11 of Halekas et al. (2017). Here we use the proton beta as a proxy for the electron beta to determine how it influences the wave occurrence rate as high electron beta conditions should lead to increased wave damping (Gary & Mellott, 1985).

3. Observations and Interpretations

Prior to exploring how the upstream parameters influence the wave occurrence rate, we must first determine whether these waves are indeed consistent with whistler mode waves. To determine this, we plot histograms for angles between the sunward direction and the wave vector θ_{kx} in Figure 3 for left-hand polarized waves and right-hand polarized waves separately. Figure 3 depicts that the left-hand polarized waves occur

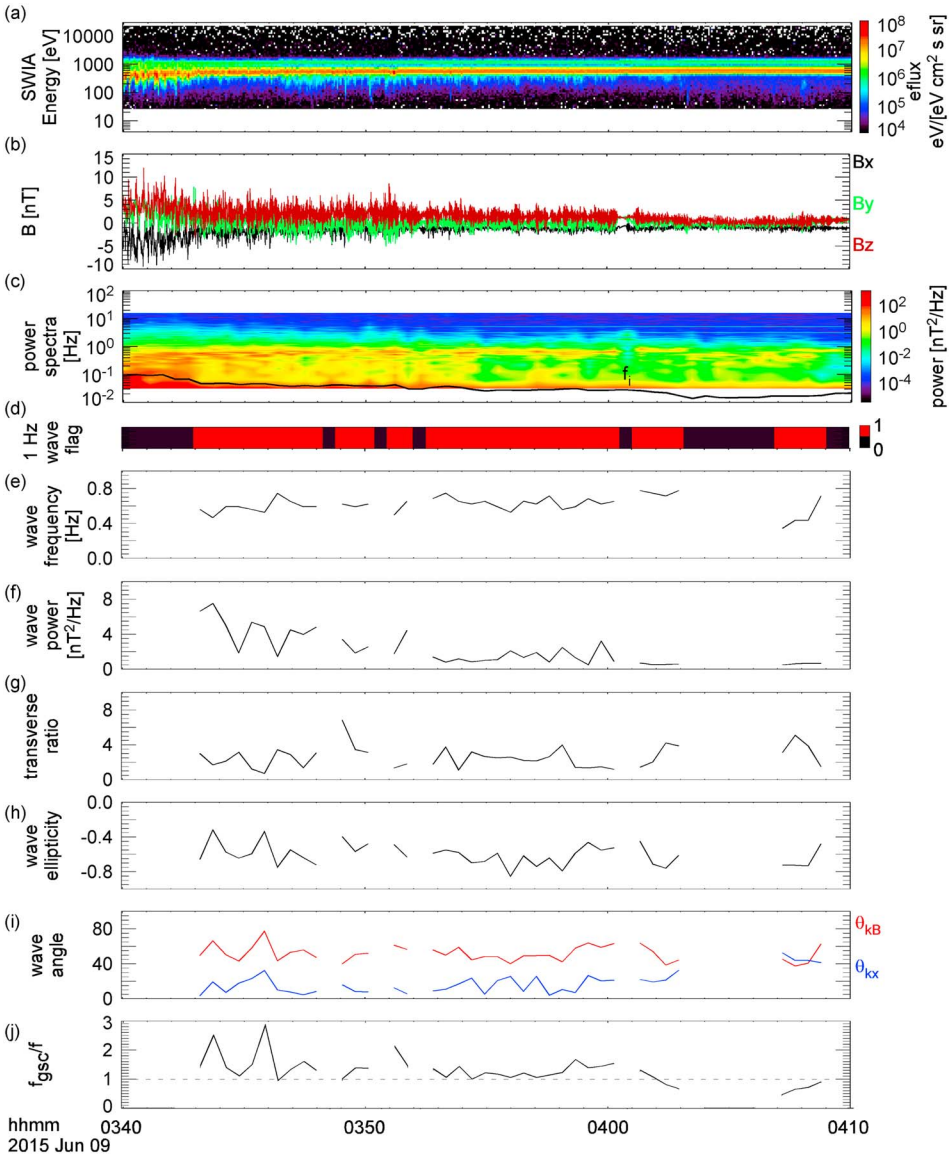

Figure 1. (a) Solar Wind Ion Analyzer energy spectrum shown to provide context for the wave observation. (b) Magnetic field time series. (c) Magnetic field power spectrum. (d) One-hertz wave flag which is the output of the automated search procedure for 1-Hz waves. Here time intervals corresponding to 1 or the red colored time intervals correspond to times where 1-Hz waves have been identified by the automated routine. (e–i) One-hertz wave parameters: frequency, power, transverse ratio, ellipticity, and wave angle. (j) The ratio of the group-standing frequency in the spacecraft frame $f_{gsc}(=\omega_{gsc}/2\pi)$ to the wave frequency in the spacecraft frame f.

preferentially for smaller θ_{kx} angles, whereas the right-hand polarized waves occur at larger θ_{kx} angles near 90°. These are the same trends seen by Brain et al. (2002) in his survey of 1-Hz waves using Mars Global Surveyor data which led them to suggest that the 1-Hz waves are in fact consistent with whistler mode waves which are intrinsically right-hand polarized. These right-hand polarized waves that have smaller θ_{kx} angles undergo maximum Doppler shift due to the solar wind convection and are seen in the spacecraft frame as left-hand polarized waves, whereas waves that propagate at large θ_{kx} angles undergo minimal Doppler shift and are seen in their intrinsic right-hand polarized state. Thus, our observations also show that the 1-Hz waves at Mars are consistent with whistler mode waves.

To determine how the upstream parameters such as the EUV flux, Mach number, and proton beta influence the 1-Hz wave occurrence rate, we plot orbit maps for the wave occurrence rates for high and low values of these parameters (see Figures 4a and 4b, 5a and 5b, and 6a and 6b). The median wave occurrence rates along

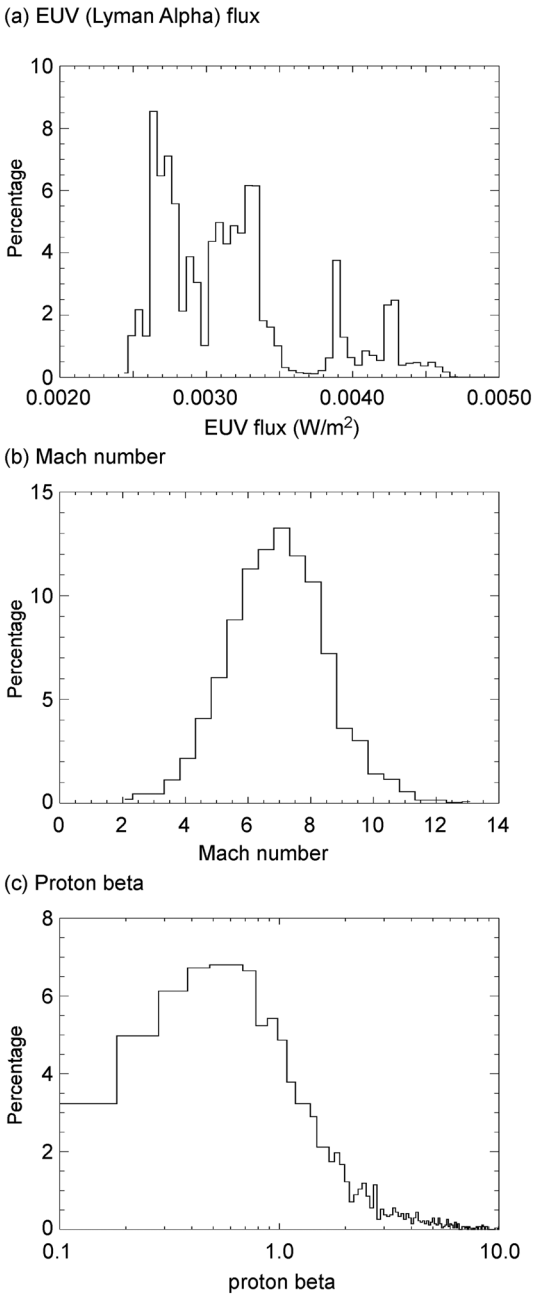

Figure 2. Histograms for upstream parameters: (a) Extreme ultraviolet flux, (b) Mach number, and (c) proton beta.

with their upper and lower quartiles are also shown in these figures corresponding to high and low values of the upstream parameters (see Figures 4c, 5c, and 6c). We find that the wave occurrence rates are significantly different only for the case of high versus low EUV flux levels (see Figures 4a and 4b). In particular, we find that the wave occurrence rates are lower for high EUV flux levels than for the low EUV flux levels.

Now we will determine the reason for the observation of the low occurrence rates of 1-Hz waves for high EUV flux levels. Halekas et al. (2017) demonstrated that the hydrogen exosphere closely tracks with the EUV flux with a maximum occurring when the EUV flux levels are the highest. A high-hydrogen exospheric density should subsequently lead to a high density in newly born pickup protons (Yamauchi et al., 2015), which can generate waves via mechanisms such as resonance (Mazelle et al., 2004). However, if these newly born pickup protons are responsible for the generation of 1-Hz waves, we should observe high wave occurrence rates

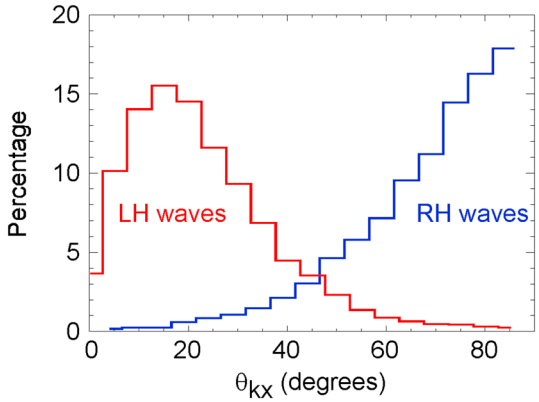

Figure 3. Histograms for the angles between the sunward direction and the wave vector θ_{kx} for left- and right-hand polarized waves separately. The preference for the observed left-hand polarized wave to have smaller θ_{kx} angles and the right-hand polarized waves to have larger θ_{kx} angles indicate that the 1-Hz waves at Mars are consistent with whistler mode waves, which are intrinsically right-hand polarized in the solar wind frame.

for high EUV flux levels, not low occurrence rates as we observe. Thus, we require a different explanation to describe the observed dependence of the wave occurrence rates with the EUV flux levels.

Tsugawa et al. (2014) suggested that the 1-Hz waves at the Moon tend to have higher power and narrower spectra when the angle between the magnetic field and the solar wind velocity θ_{BV} is small while the waves tend to have lower power and broader spectra when θ_{BV} is large. Thus, can the observed wave occurrence rate dependence with the EUV flux levels be a consequence of times corresponding to low and high EUV fluxes having different θ_{BV} distributions? To answer this, we plot the distributions of θ_{BV} for high and low EUV flux conditions in Figure 7 and we find that the θ_{BV} distributions are comparable for both the high and low EUV flux conditions. Thus, the observed wave occurrence rate dependence with the EUV flux levels is not a consequence of θ_{BV} having different distributions for times with low and high EUV flux levels.

We hypothesize that the 1-Hz waves are masked by enhanced turbulence levels due to an enhanced occurrence rate of lower-frequency proton cyclotron waves, which become prominent during the times of high EUV flux levels. Romanelli et al. (2016) observed this enhancement in the occurrence rate of the proton cyclotron waves near Mars's perihelion where the EUV flux levels are high. Turbulence levels at higher frequencies can be enhanced by low-frequency waves resulting from a turbulent cascade of energy (Tsurutani et al., 1995). Such energy cascade processes have been previously reported in the upstream region of Mars (Ruhunusiri et al., 2017). To demonstrate this enhancement in turbulence during times with high EUV flux levels, we plot the median power spectra for the upstream magnetic field fluctuations in Figure 8 for frequencies between $3f_i$ (which has a median value near 0.1 Hz) and 3 Hz, where we searched for the 1-Hz waves for high and low EUV flux levels separately. Figure 8 depicts that the turbulence levels are considerably higher during the times with high EUV flux levels than during the times with low EUV flux levels. This enhanced turbulence during the times with high EUV flux levels can lead to masking of the 1-Hz waves, leading to an apparent reduction in the 1-Hz wave occurrence rate during those times.

To demonstrate that the 1-Hz wave occurrence rate is indeed influenced by the low-frequency turbulence levels, we compute the mean power spectral density for frequencies less than $3f_i$ and plot 1-Hz wave occurrence rate orbit maps for high and low values of the mean power spectral density in that frequency range in Figure 9. The median low-frequency turbulence level is 2.6 nT^2/Hz. Thus, turbulence values of 1.2 nT^2/Hz and 4.9 nT^2/Hz are selected surrounding this median value to bin observational data into low versus high turbulence levels. We find that the wave occurrence rates are significantly lower for high turbulence levels than for the low turbulence levels indicating that the wave masking leads to an apparent reduction of 1-Hz wave occurrence rate. Similar observations have been made recently for whistler mode waves in the solar wind. For example, a recent investigation of whistler mode waves in the solar wind by Lacombe. et al. (2014) have revealed that a low level of background turbulence is one of the necessary conditions for the observation of these waves. Lacombe. et al. (2014) suggested that this is a consequence of masking of whistler mode waves by background turbulence when the background turbulence levels are high.

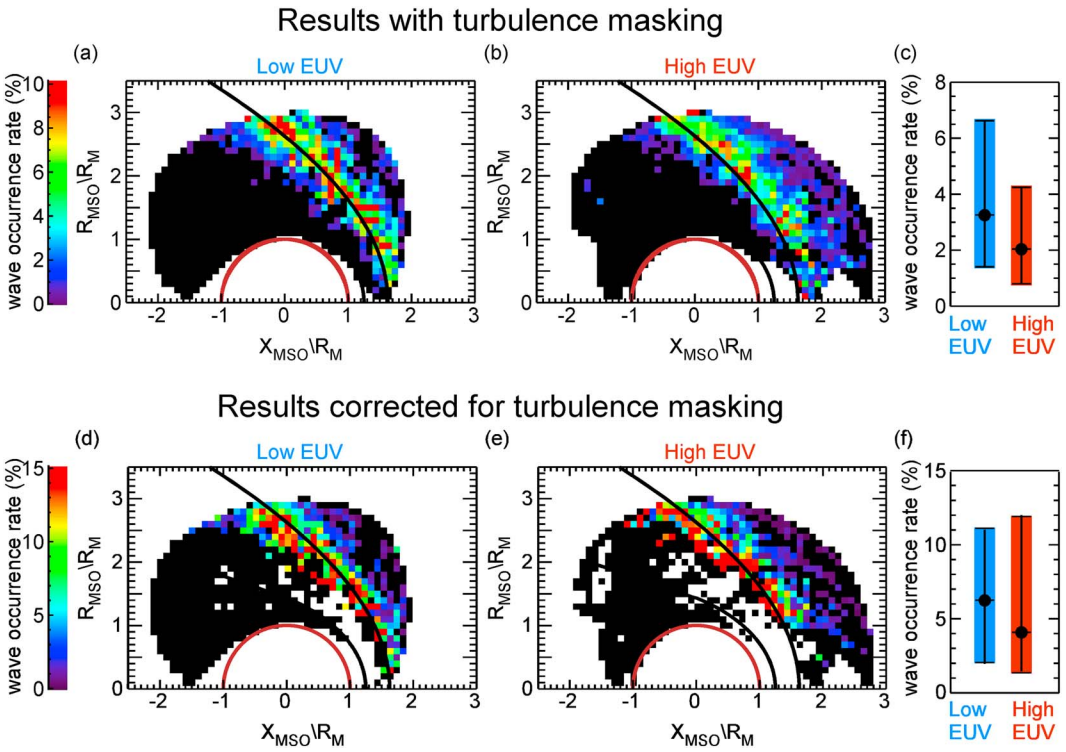

Figure 4. (a, b) Orbit maps for the 1-Hz wave occurrence rates for low (<0.0027 W/m^2) and high (>0.0032 W/m^2) extreme ultraviolet (EUV) flux levels. (c) Median wave occurrence rates and lower and upper quartiles for the low and high EUV flux levels. (d, e) Orbit maps for the 1-Hz wave occurrence rates for low (<0.0027 W/m^2) and high (>0.0032 W/m^2) EUV flux levels under low turbulent conditions (<1.2 nT^2/Hz). (f) Median wave occurrence rates and lower and upper quartiles for the low and high EUV flux levels under the low turbulent conditions. Note that the results shown in (a)–(c) have not been corrected for turbulence masking effects, whereas results shown in (d)–(f) have been corrected for turbulence masking effects. The turbulence masking corrected results shown in (d)–(f) reveal that the wave occurrence rates do not vary significantly with the EUV flux levels. MSO = Mars Solar Orbital.

Turbulent masking can also preclude the identification of any intrinsic dependencies of the wave occurrence rate with upstream parameters. This can be the reason as to why we did not observe a significant change of the wave occurrence rate with the high and low values of Mach numbers and proton beta values as can be seen in panels a and b in Figures 5 and 6, respectively.

To determine the dependencies of the wave occurrence rates on the upstream parameters excluding the biases due to wave masking effects, we plot the wave occurrence rate orbit maps for high and low values of EUV flux levels, Mach numbers, and proton beta values only selecting time segments with low values of low-frequency background turbulence in panels d and e of Figures 4–6. We find that the wave occurrence rates for both the low and high EUV flux levels under low turbulence levels are comparable (see Figures 4d–4f). The absence of a significant dependence of the wave occurrence rate with the EUV flux levels indicates that the newly born pickup ions produced in Mars's exosphere contribute minimally to the generation of 1-Hz waves. We find that the 1-Hz wave occurrence rates are higher for the low Mach numbers than for the high Mach numbers under low turbulent conditions (see Figures 5d–5f). We also find that the 1-Hz wave occurrence rates are higher for low proton beta values than for the high proton beta values under low turbulent conditions (see Figures 6d–6f).

To aid us in the identification of the mechanism behind the observed dependencies of the wave occurrence rates with the Mach numbers and proton beta values, we plot distributions of wave parameters such as the wave frequency, power, transverse ratio, ellipticity, and θ_{kB} for high and low values of Mach numbers and proton beta values under low turbulent conditions in Figures 10 and 11. We find that the frequencies of 1-Hz waves are biased toward lower values for the low Mach numbers than for the high Mach numbers (see Figure 10a). We also find that the percentage of low-amplitude waves are higher for the high Mach number conditions than for the low Mach number conditions (see Figure 10b). The distributions for transverse ratio,

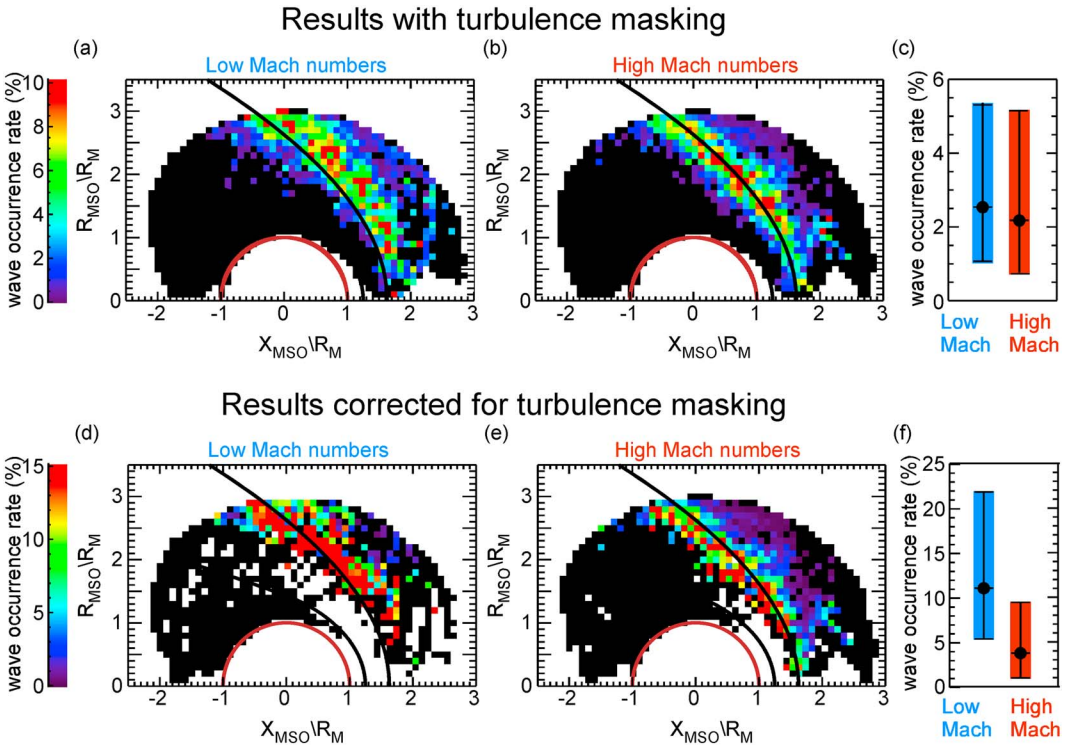

Figure 5. (a, b) Orbit maps for the 1-Hz wave occurrence rates for low (<6.1) and high (>8.0) magnetosonic Mach numbers. (c) Median wave occurrence rates and lower and upper quartiles for the low and high Mach numbers. (d, e) Orbit maps for the 1-Hz wave occurrence rates for low (<6.1) and high (>8.0) magnetosonic Mach numbers under the low turbulent conditions (<1.2 nT^2/Hz). (f) Median wave occurrence rates and lower and upper quartiles for the low and high Mach numbers under the low turbulent conditions. Note that the results shown in (a)–(c) have not been corrected for turbulence masking effects, whereas results shown in (d)–(f) have been corrected for turbulence masking effects. The turbulence masking corrected results shown in (d)–(f) reveal that the wave occurrence rates are higher for the low Mach numbers than for the high Mach numbers. MSO = Mars Solar Orbital.

ellipticity, and θ_{kB}, for both low and high Mach number conditions, are comparable. We find that the wave frequencies tend to be lower for the low proton beta values than for the high proton beta values (see Figure 11a). The wave parameters such as wave power, transverse ratio, ellipticity, and θ_{kB} have comparable distributions for both the low and high values of proton beta.

Investigations of 1-Hz wave at Mercury have revealed that the wave amplitudes are much larger than those at Earth (Le et al., 2013). Since the upstream Mach numbers at Mercury are relatively lower than those at Earth, Le et al. (2013) suggested that this is indicative of low Mach number conditions being preferred over high Mach number conditions for the generation of 1-Hz waves. Our observations of the high occurrence rate of 1-Hz waves for the low Mach number conditions than for the high Mach number conditions along with the observation of the low percentage of low-amplitude 1-Hz waves for low Mach number conditions are consistent with these previous interpretations that the 1-Hz waves are likely to be generated under low Mach number conditions. If the waves are likely to be generated under the low Mach number conditions, it rules out reflected particles from the bow shock as a dominant source for the generation of 1-Hz waves at Mars, as low Mach numbers lead to a lower proportion of reflected particles from the bow shock. Our observation of the low occurrence rate of 1-Hz wave for high proton beta values (which is a proxy for electron beta values) is consistent with enhanced Landau damping of waves at high electron beta values (Gary & Mellott, 1985).

The observed dependencies of the wave occurrence rate with the Mach numbers and beta values may not be necessarily related to the dependence of the wave generation mechanism or damping with these parameters as interpreted above. Instead, it is possible that this dependence may have to do with the observability of waves in the spacecraft frame. While the 1-Hz waves appear monochromatic in the spacecraft frame, they may not be necessarily monochromatic in the plasma frame. In fact, broadband waves that satisfy a group-standing condition, in which the component of the wave group velocity parallel to the solar wind flow

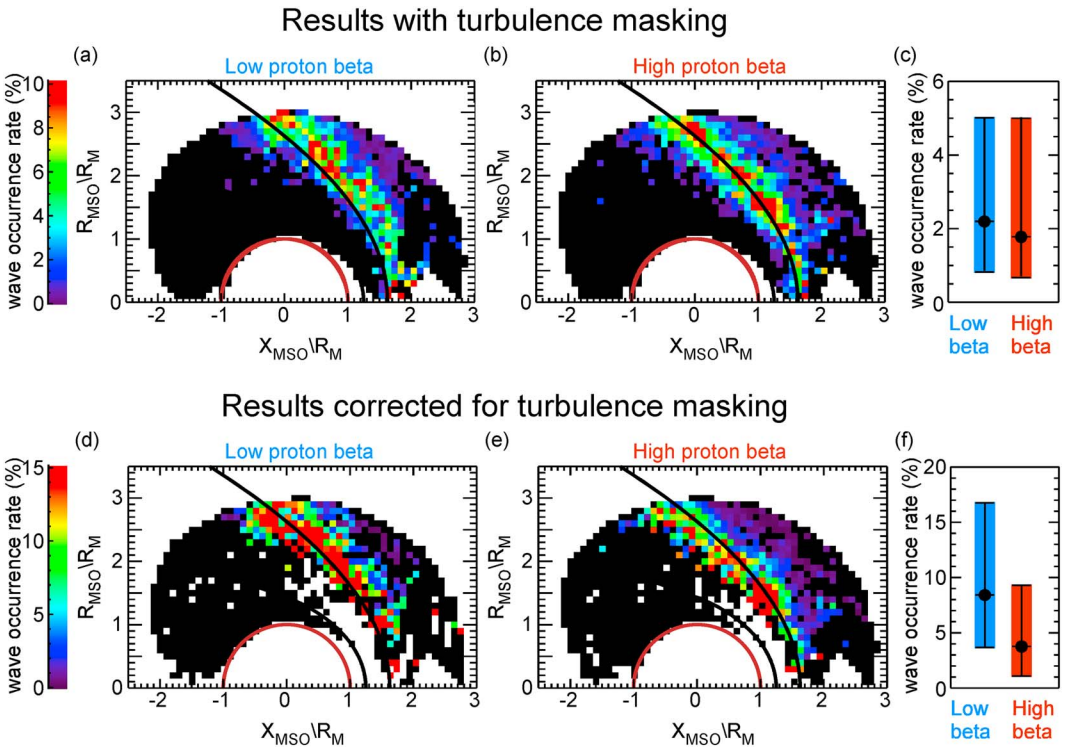

Figure 6. (a, b) Orbit maps for the 1-Hz wave occurrence rates for low (<0.6) and high (>1.7) proton beta values. (c) Median wave occurrence rates and lower and upper quartiles for the low and high proton beta values. (d, e) Orbit maps for the 1-Hz wave occurrence rates for low (<0.6) and high (>1.7) proton beta values under the low turbulent conditions (<1.2 nT^2/Hz). (f) Median wave occurrence rates and lower and upper quartiles for the low and high proton beta values under the low turbulent conditions. Note that the results shown in (a)–(c) have not been corrected for turbulence masking effects, whereas results shown in (d)–(f) have been corrected for turbulence masking effects. The turbulence masking corrected results shown in (d)–(f) reveal that the wave occurrence rates are higher for the low proton beta values than for the high proton beta values. MSO = Mars Solar Orbital.

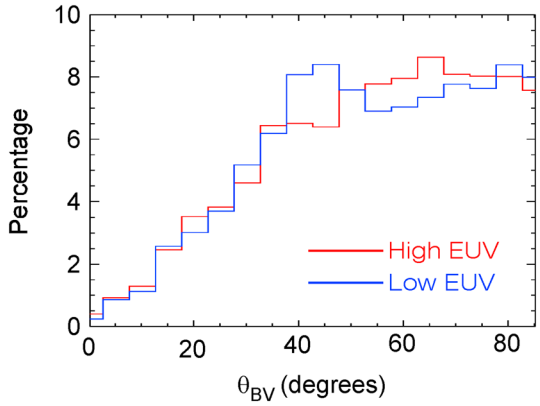

Figure 7. Distributions for the angle between the magnetic field and the solar wind velocity θ_{BV} for times corresponding to low (<0.0027 W/m^2) and high (>0.0032 W/m^2) extreme ultraviolet (EUV) flux levels. The θ_{BV} distributions corresponding to the low and high EUV flux levels are comparable. This indicates that the observed wave occurrence rate trend with the EUV flux levels seen in Figures 4a and 4b is not a consequence of any θ_{BV} distribution differences between the times with low and high EUV flux levels.

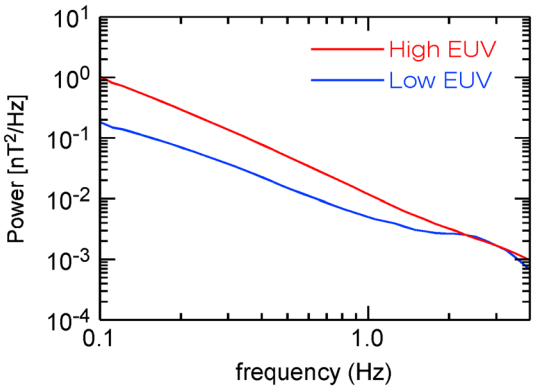

Figure 8. Median turbulence spectra for low (<0.0027 W/m^2) and high (>0.0032 W/m^2) extreme ultraviolet flux levels. The turbulent levels are high during the times of high extreme ultraviolet flux, enabling masking of the 1-Hz waves.

velocity becomes equal or becomes nearly equal to the solar wind flow velocity, can appear monochromatic and highly peaked (in a power spectrum) in the spacecraft frame due to Doppler shift (Tsugawa et al., 2014). The group-standing condition is a function of the solar wind velocity, magnetic field, solar wind density, angle between the wave vector and the magnetic field, and the angle between the wave vector and the sunward direction (Tsugawa et al., 2014). Thus, the observed wave occurrence rate dependence with the Mach numbers and beta values can be a consequence of how the group-standing condition is satisfied for different Mach numbers and proton beta values. An evidence in favor of this is that at both the low Mach numbers and low proton beta values, where we observe a high occurrence rate of waves, we find that the wave frequencies tend to be lower. If the group-standing condition leads to the appearance of waves in the spacecraft frame at lower frequencies, the waves tend to appear highly peaked than if they appear at higher frequencies (Tsugawa et al., 2014).

In order to determine whether the 1-Hz waves at Mars satisfy the group-standing condition, the ratio of the group-standing frequency to the wave frequency in the spacecraft frame needs to be computed. If this ratio is nearly equal to 1, then a wave satisfies the group-standing condition. To compute the group-standing frequency, we start with the whistler wave dispersion relation from Fairfield (1974): $c^2k^2/\omega_0 = -\omega_{pe}^2/(\omega_0 - \Omega_e \cos\theta_{kB})$, where ω_0 is the wave frequency in the plasma frame or the solar wind frame, Ω_e is the electron gyrofrequency, and c is the speed of light. The group velocity of the wave which is derived from this equation is $V_g = \frac{c}{\omega_{pe}}[\omega_0(\Omega_e \cos\theta_{kB} - \omega_0)]^{1/2}\left(2(\Omega_e \cos\theta_{kB} - \omega_0)\hat{k}/\Omega_e \cos\theta_{kB} - \tan\theta_{kB}\hat{\theta}\right)$, where $\hat{k}$ is the unit wave vector and $\hat{\theta}$ is a unit vector perpendicular to $\hat{k}$ (see equation (3) in Fairfield, 1974). We determine the group-standing frequency ω_{g0} in the plasma frame numerically by solving $V_{sw} - V_g \cdot \hat{V}_{sw} = 0$ where $\hat{V}_{sw}$ is the unit vector

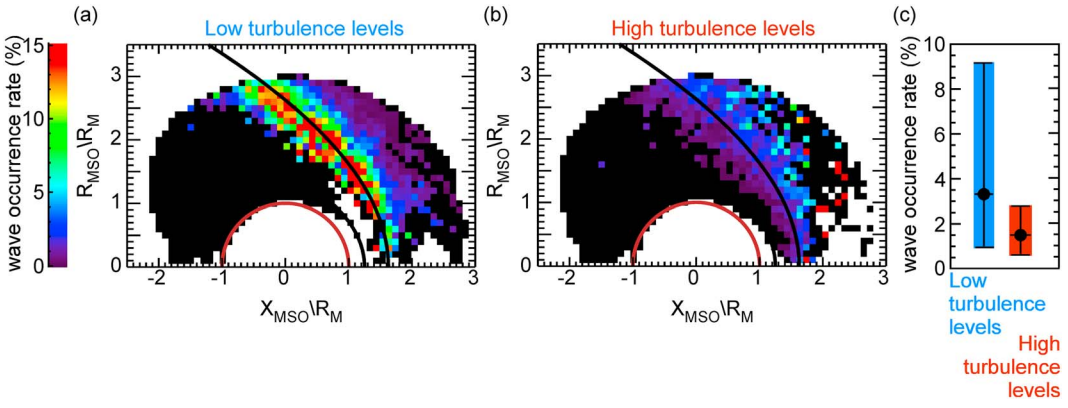

Figure 9. (a, b) Orbit maps for the 1-Hz wave occurrence rates for low (<1.2 nT^2/Hz) and high (>4.9 nT^2/Hz) turbulence levels. (c) Median wave occurrence rates and lower and upper quartiles for the low and high turbulence levels. The wave occurrence rate is significantly lower for the high turbulence levels than for the low turbulence levels indicating masking of waves under high turbulent conditions. MSO = Mars Solar Orbital.

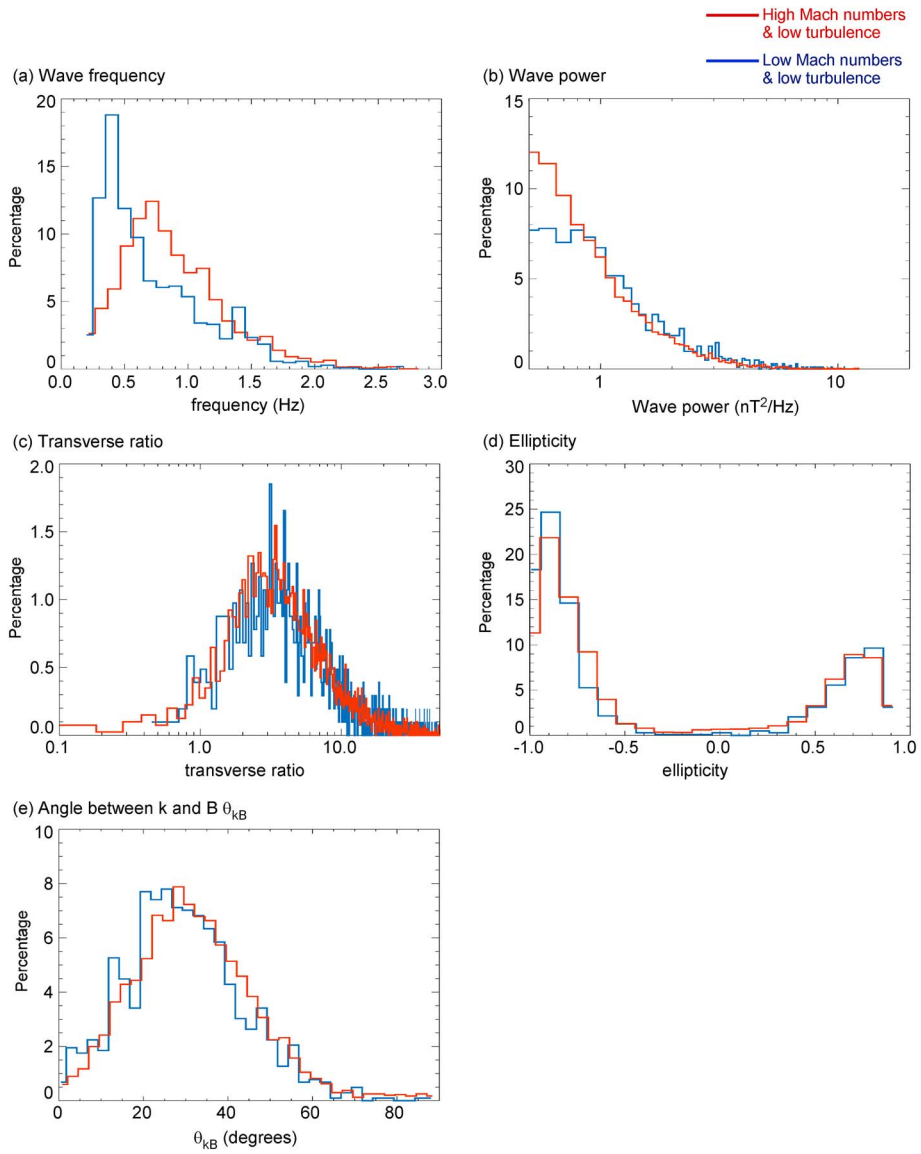

Figure 10. (a–e) Histograms of 1-Hz wave characteristics for low (<6.1) and high (>8.0) Mach numbers under low turbulent conditions (<1.2 nT^2/Hz): frequency, power, transverse ratio, ellipticity, and the angle between the wave vector k and the magnetic field B, θ_{kB}. The wave frequencies tend to be lower for the low Mach numbers than for the high Mach numbers.

in the direction of the solar wind. Then, we find the wave vector k_g associated with this frequency from the whistler wave dispersion relation. Finally, we find the group-standing frequency in the spacecraft frame ω_{gsc} by using the Doppler shift equation $\omega_{gsc} = \omega_{g0} + k_g \cdot V_{sw}$. We plot the ratio of the group-standing frequency in the spacecraft frame computed in this manner to the observed wave frequency in the spacecraft frame for the example wave shown in Figure 1j. As can be seen in Figure 1j, this ratio is nearly equal to 1, and this indicates that the example wave shown in Figure 1, in fact, satisfies the group-standing condition.

We compute this ratio for the 1-Hz waves identified for all the low turbulent conditions and plot a histogram of this ratio in Figure 12. We find that a high percentage of the waves have a ratio nearly equal to 1 implying that a large fraction of the waves satisfy the group-standing condition. This suggest that a large fraction of 1-Hz waves that are seen as monochromatic waves in the spacecraft frame may not be monochromatic waves in the solar wind frame, but rather, they may have a broad distribution of frequencies.

Now we will determine how the group-standing frequency varies with the Mach number and proton beta. For this, we first compute the group-standing frequency for median upstream and wave parameters.

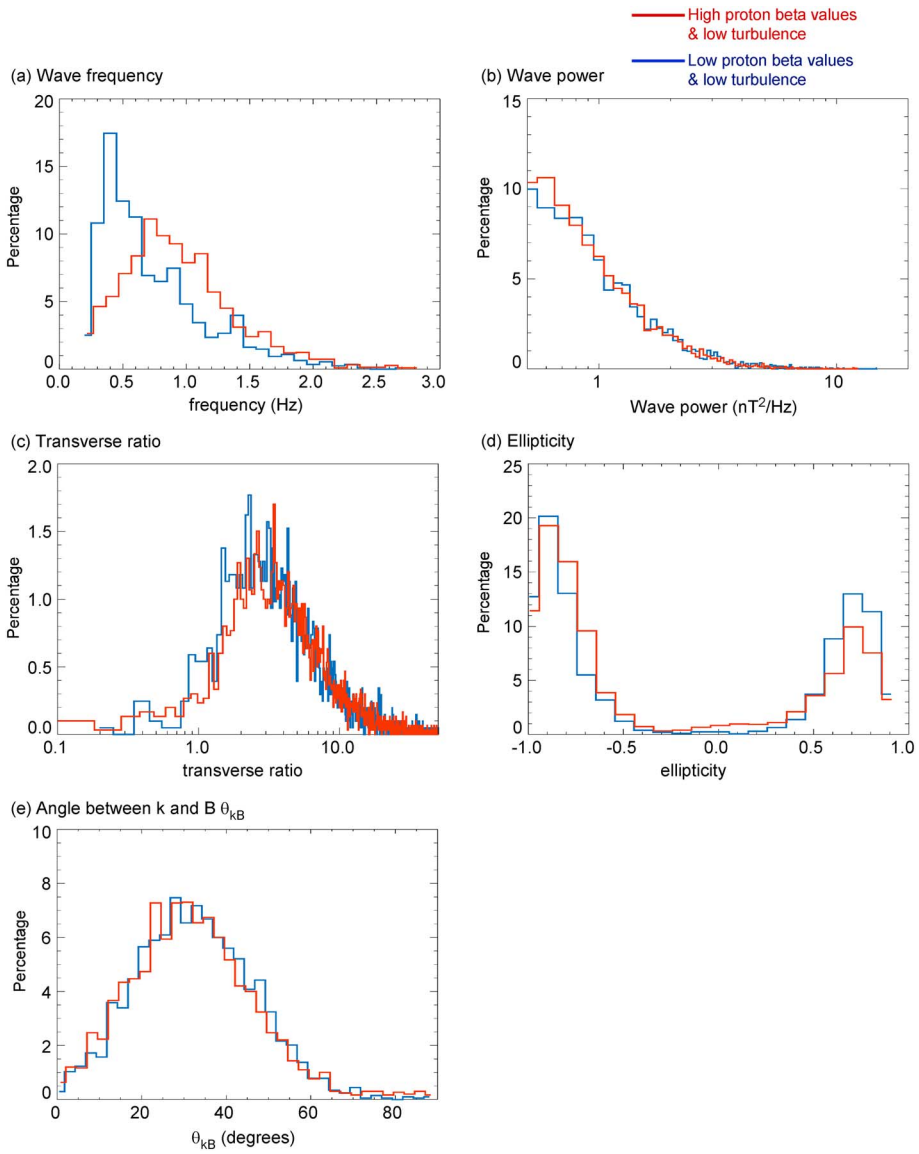

Figure 11. (a, e) Histograms of 1-Hz wave characteristics for low (<0.6) and high (>1.7) beta values under low turbulent conditions (<1.2 nT^2/Hz): frequency, power, transverse ratio, ellipticity, and the angle between the wave vector k and the magnetic field B, θ_{kB}. The wave frequencies tend to be lower for the low proton beta values than for the high proton beta values.

Then, we vary these parameters to correspond to increasing or decreasing Mach numbers or proton beta values to determine how the group-standing frequency varies. This calculation reveals that the group-standing frequency decreases when decreasing either the Mach number or the proton beta (see Table 1). As noted previously, we observe that at both the low Mach numbers and low proton beta values the wave frequencies tend to be smaller (see Figures 10a and 11a). Since we determined that a large percentage of the 1-Hz waves satisfy the group-standing condition, this observed wave frequency trends are consistent with what is expected from the group-standing condition. The lower the group-standing frequency, the wave becomes more peaked aiding it to be observable (Tsugawa et al., 2014) and leading the waves to have a high occurrence rate corresponding to those conditions. Thus, the observed wave occurrence rate variations with the Mach number and proton beta, seen in Figures 5d–5f and 6d–6f, are consistent with how the group-standing condition varies with the Mach number and proton beta.

We find that the wave occurrence rates in both the quasi-parallel and quasi-perpendicular foreshock regions are comparable under low turbulent conditions. This result is obtained by plotting R_{MSE} $(= \sqrt{Y_{MSE}^2 + Z_{MSE}^2})$

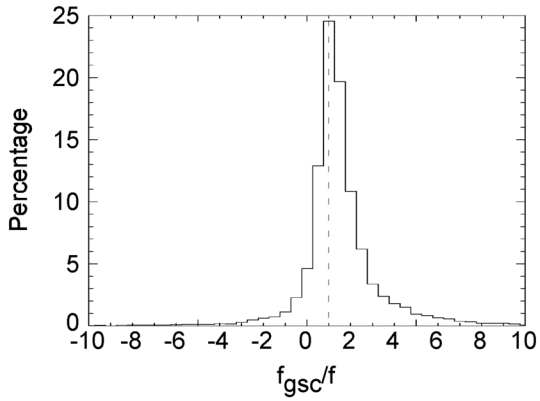

Figure 12. Histograms for the ratio of the group-standing frequency in the spacecraft frame $f_{gsc}(=\omega_{gsc}/2\pi)$ to the wave frequency in the spacecraft frame f for 1-Hz waves at Mars under low turbulent conditions (<1.2 nT^2/Hz). A high percentage of the waves have a ratio near 1 indicating that a large fraction of the 1-Hz waves at Mars satisfy the group-standing condition.

versus X_{MSE} maps shown in Figure 13 for low turbulent conditions. The quasi-parallel foreshock region is the region where the angle between the upstream magnetic field and the bow shock normal becomes small (typically <30°), whereas the quasi-perpendicular foreshock region is where the angle between the upstream magnetic field and the bow shock normal is large (typically >60°). Here MSE stands for the Mars Solar Electric coordinate system in which the X_{MSE} axis is aligned antiparallel to the direction of the dominant solar wind flow, Y_{MSE} axis is directed along the upstream magnetic field perpendicular to the solar wind flow, and Z_{MSE} axis points along the upstream convective electric field. While the nominal Parker interplanetary magnetic field orientation is 56° to the Mars-Sun line at Mars, MAVEN observations have shown that the magnetic field orientation can take a range of values, with a majority lying between 40° and 140° (Ruhunusiri et al., 2017),

Table 1
Comparison of the Group-Standing Frequencies for High Versus Low Mach Numbers and Proton Beta

B (nT)	n (cm^{-3})	Mach number	f_{gsc} (Hz)
3.5	2.2	6.0	0.3
2.7	2.2	6.9	0.4
1.5	2.2	8.3	0.7
2.7	1.3	6.0	0.2
2.7	2.2	6.9	0.4
2.7	7.2	8.3	1.2
B (nT)	n (cm^{-3})	Proton beta	f_{gsc} (Hz)
3.8	2.2	0.3	0.3
2.7	2.2	0.6	0.4
1.5	2.2	1.9	0.7
2.7	1.1	0.3	0.2
2.7	2.2	0.6	0.4
2.7	6.9	1.9	1.1

Notes. The group-standing frequencies are determined using median values of upstream parameters and wave parameters: proton density $n = 2.2$ cm^{-3}, $B = 2.7$ nT, $\theta_{kB} = 35°$, $\theta_{kV} = 133°$. To determine how the group-standing frequency varies with the Mach number and the proton beta, we determine the group-standing frequency by varying either the magnetic field or the proton density, keeping the other fixed since both Mach number and the proton beta are functions of the magnetic field and the proton density. To compute the Mach numbers and proton beta values, we also used a median proton temperature of $T = 7.7$ eV. We find that the group-standing frequency decreases with decreasing Mach number and proton beta.

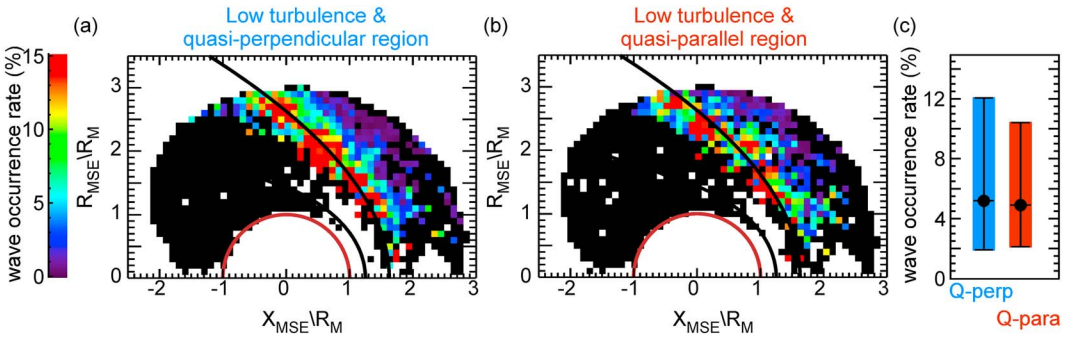

Figure 13. (a, b) R_{MSE} versus X_{MSE} maps depicting the occurrence rate of the 1-Hz waves in the quasi-perpendicular and quasi-parallel foreshock regions under low turbulent conditions (<1.2 nT^2/Hz). (c) Median wave occurrence rates and lower and upper quartiles for the quasi-perpendicular and quasi-parallel foreshock regions, respectively. The wave occurrence rates are comparable in the quasi-perpendicular and quasi-parallel regions. MSE = Mars Solar Electric.

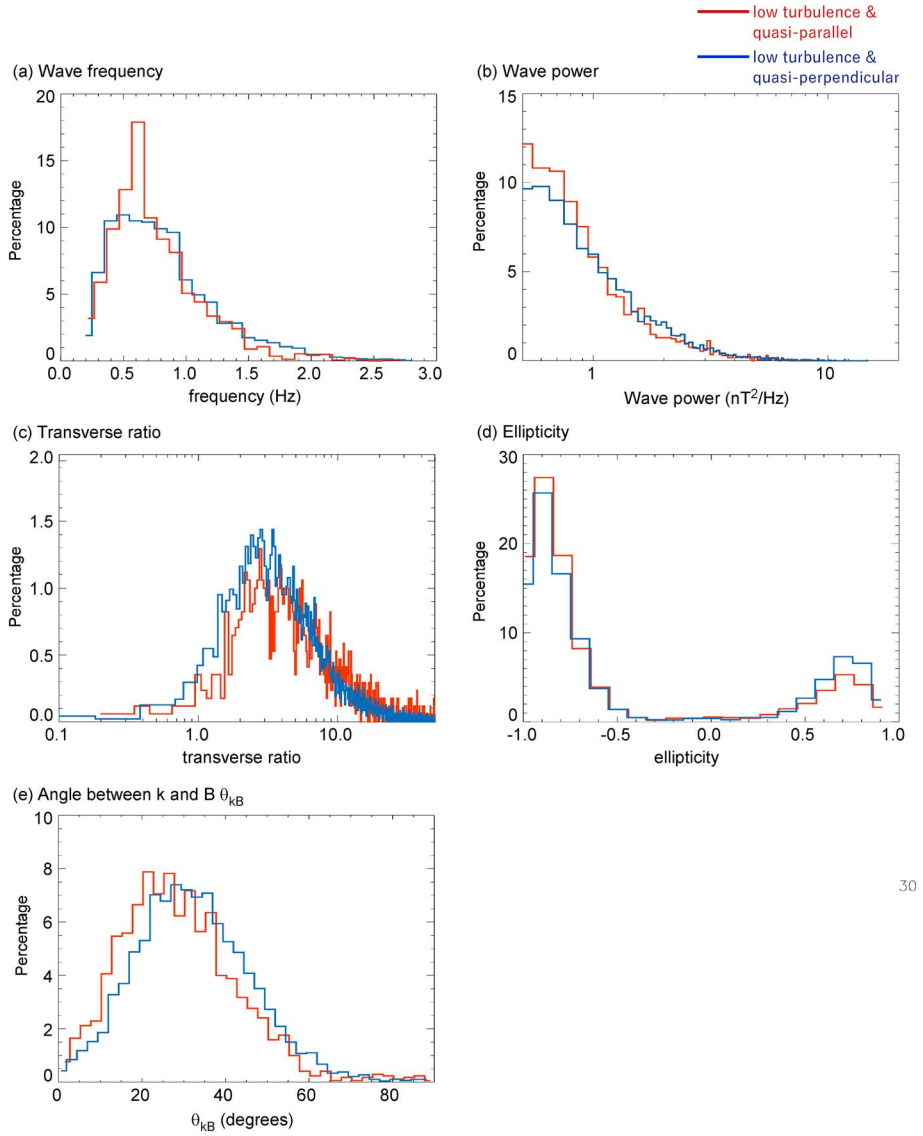

Figure 14. (a–e) Histograms of 1-Hz wave parameters for quasi-parallel and quasi-perpendicular regions under low turbulent conditions (<1.2 nT^2/Hz): frequency, power, transverse ratio, ellipticity, and θ_{kB}. The wave frequency distribution tends to be slightly broader in the quasi-perpendicular region than in the quasi-parallel region.

due to solar wind stream-stream interactions. This enables us to determine the wave occurrence rates in both the quasi-parallel and quasi-perpendicular foreshock regions for varying angles between the solar wind velocity and the magnetic field. In the MSE orbit plot maps, when $B_x > 0$ or when the upstream magnetic field is facing sunward, the quasi-parallel foreshock region is located in the $Y_{MSE} > 0$ region, whereas the quasi-perpendicular foreshock region is located in the $Y_{MSE} < 0$ region. When $B_x < 0$ or when the upstream magnetic field is facing antisunward, the quasi-parallel foreshock is located in the $Y_{MSE} < 0$ region, whereas the quasi-perpendicular foreshock is located in the $Y_{MSE} > 0$ region. Thus, to determine the wave occurrence rates in the quasi-perpendicular foreshock region, we plot wave occurrence rates in a R_{MSE} versus X_{MSE} map by requiring that $B_x > 0$, $Y_{MSE} < 0$, and the cone angle θ_{Bx} be less than 60° or $B_x < 0$, $Y_{MSE} > 0$, and $120° < \theta_{Bx} < 180°$, during the wave observations (see Figure 13a). Similarly, to determine the wave occurrence rates in the quasi-parallel foreshock region, we plot wave occurrence rates in a R_{MSE} versus X_{MSE} map by requiring that $B_x > 0$, $Y_{MSE} > 0$, and $0° < \theta_{Bx} < 60°$ or $B_x < 0$, $Y_{MSE} < 0$, and $120° < \theta_{Bx} < 180°$, during the wave observations (see Figure 13b). Comparison of Figures 13a and 13b reveals that the wave occurrence rates are similar in both the quasi-perpendicular and quasi-parallel foreshock regions.

Inspection of wave parameters in the quasi-parallel and quasi-perpendicular foreshock region under low turbulent conditions reveals that the distribution of wave frequencies tends to be slightly broader in the quasi-perpendicular region than in the quasi-parallel region (see Figure 14a). The other wave parameters have comparable distributions in both the quasi-parallel and quasi-perpendicular foreshock regions (see Figures 14b–14e).

4. Summary

We used a Martian year of MAVEN spacecraft observations to characterize 1-Hz waves at Mars. We find that the wave occurrence rate becomes lower for high turbulence levels indicative of wave masking by background turbulence. Similar turbulence masking can also affect identification of such waves elsewhere in the solar system. Thus, the severity of turbulence masking should be assessed in future investigations of 1-Hz waves in other planetary bodies and the Moon.

Survey of wave occurrence rates for the low turbulence conditions revealed that the wave occurrence rate is the same for both the high and low EUV conditions indicating that pickup ions from Mars's extended exosphere contribute minimally to the 1-Hz wave generation. We find that the wave occurrence rate becomes higher for the low Mach numbers than for the high Mach numbers. We also find that the wave frequencies tend to be lower for the low Mach numbers than for the high Mach numbers. We infer that the observed dependence of the wave occurrence rate with the Mach numbers can be a consequence of the low Mach number conditions being preferred for wave generation over high Mach numbers or a consequence of how Mach numbers influence the group-standing condition of the waves. We find a low occurrence rate of waves for the high proton beta values. We also find that the wave frequencies tend to be lower for the low proton beta values than for the high proton beta values. Based on these observations, we infer that the dependence of wave occurrence rate with the proton beta values can be a consequence of Landau damping of waves, which become prominent for high beta values or a consequence of how proton beta values influence the group-standing condition. We observe that the 1-Hz waves are equally likely to be found in both the quasi-parallel and quasi-perpendicular foreshock regions. However, the frequency distribution of the waves in the quasi-perpendicular region is slightly broader than that in the quasi-parallel region.

Acknowledgments
This work was supported by NASA. C. Mazelle was supported by CNES. We thank J. E. P. Connerney for MAG data. MAVEN data are publicly available through the Planetary Data System.

References

Balikhin, M. A., Dudok de Witt, T., Woolliscroft, L. J. C., Walker, S. N., Alleyne, H., Krasnoselskikh, V., et al. (1997). Experimental determination of the dispersion of waves observed upstream of a quasi-perpendicular shock. *Geophysical Research Letters*, *24*(7), 787–790. https://doi.org/10.1029/97GL00671

Barabash, S., & Lundin, R. (1993). Reflected ions near Mars: Phobos-2 observations. *Geophysical Research Letters*, *20*(9), 787–790. https://doi.org/10.1029/93GL00834

Bertucci, C., Achileos, N., Mazelle, C., Russell, C. T., Thomsen, M., Hospodarsky, G., et al. (2007). Low frequency waves in the foreshock of Saturn: First results from Cassini. *Journal of Geophysical Research*, *112*, A09219. https://doi.org/10.1029/2006JA012098

Bertucci, C., Mazelle, C., & Acuña, M. H. (2005). Interaction of the solar wind with Mars from Mars Global Surveyor MAG/ER observations. *Journal of Atmospheric and Terrestrial Physics*, *67*(17-18), 1797–1808. https://doi.org/10.1016/j.jastp.2005.04.007

Brain, D. A., Bagenal, F., Acuña, M. H., Connerney, J. E. P., Crider, D. H., Mazelle, C., et al. (2002). Observations of low-frequency electromagnetic plasma waves upstream from the Martian shock. *Journal of Geophysical Research*, *107*(A6), 1076. https://doi.org/10.1029/2000JD000416

Connerney, J., Espley, J., Lawton, P., Murphy, S., Odom, J., Oliversen, R., & Sheppard, D. (2015). The MAVEN magnetic field investigation. *Space Science Reviews*, *195*(1–4), 257–291. https://doi.org/10. 1007/s11214-015-0169-4

Connerney, J. E. P., Espley, J. R., DiBraccio, G. A., Gruesbeck, J. R., Oliversen, R. J., Mitchell, D. L., et al. (2015). First results of the MAVEN magnetic field investigation. *Geophysical Research Letters*, *42*, 8819–8827. https://doi.org/10.1002/2015GL065366

Curry, S. M., Liemohn, M. W., Fang, X., Brain, D., & Ma, Y. (2013). Simulated kinetic effects of the corona and solar cycle on high altitude ion transport at Mars. *Journal of Geophysical Research: Space Physics*, *118*, 3700–3711. https://doi.org/10.1002/jgra.50358

Curry, S. M., Liemohn, M. W., Fang, X., Ma, Y., Nagy, A. F., & Espley, J. (2013). The influence of production mechanisms on pickup ion loss at Mars. *Journal of Geophysical Research: Space Physics*, *118*, 554–569. https://doi.org/10.1029/2012JA017665

Delva, M., Mazelle, C., & Bertucci, C. (2011). Upstream ion cylotron waves at Venus and Mars. *Space Science Reviews*, *162*, 5–24. https://doi.org/10.1007/s11214-011-9828-2

Eparvier, F. G., Chamberlin, P. C., Woods, T. N., & Thiemann, E. M. B. (2015). The solar extreme ultraviolet monitor for MAVEN. *Space Science Reviews*, *195*(1–4), 293–301. https://doi.org/10.1007/s11214-015-0195-2

Fairfield, D. H. (1974). Whistler waves observed upstream from collisionless shocks. *Journal of Geophysical Research*, *79*(10), 1368–1378. https://doi.org/10.1029/JA079i010p01368

Fairfield, D. H., & Behannon, K. W. (1976). Bow shock and magnetosheath waves at Mercury. *Journal of Geophysical Research*, *81*(22), 3897–3906. https://doi.org/10.1029/JA081i022p03897

Feldman, W. C., Anderson, R. C., Bame, S. J., Gary, S. P., Gosling, J. T., McComas, D. J., et al. (1983). Electron velocity distributions near the Earth's bow shock. *Journal of Geophysical Research*, *88*(A1), 96–110. https://doi.org/10.1029/JA088iA01p00096

Gary, S. P., & Mellott, M. M. (1985). Whistler damping at oblique propagation: Laminar shock precursors. *Journal of Geophysical Research*, *90*(A1), 99–104. https://doi.org/10.1029/JA090iA01p00099

Greenstadt, E. W., Le, G., & Strangeway, R. J. (1995). ULF waves in the foreshock. *Advances Space Research*, *15*(8–9), 71–84. https://doi.org/10.1016/0273-1177(94)00087-H

Gurgiolo, C., Wong, H. K., & Winske, D. (1993). Low and high frequency waves generated by gyrophase bunched ions at oblique shocks. *Geophysical Research Letters*, *20*(9), 783–786. https://doi.org/10.1029/93GL00854

Halekas, J. S., Brain, D. A., Mitchell, D. L., & Lin, R. P. (2006). Whistler waves observed near lunar crustal magnetic sources. *Geophysical Research Letters*, *33*, L22104. https://doi.org/10.1029/2006GL027684

Halekas, J. S., Poppe, A. R., McFadden, J. P., & Glassmeier, K.-H. (2013). The effects of reflected protons on the plasma environment of the moon for parallel interplanetary magnetic fields. *Geophysical Research Letters*, *40*, 4544–4548. https://doi.org/10.1002/grl.50892

Halekas, J. S., Ruhunusiri, S., Harada, Y., Collinson, G., Mitchell, D. L., Mazelle, C., et al. (2017). Structure, dynamics, and seasonal variability of the Mars-solar wind interaction: MAVEN solar wind ion analyzer in-flight performance and science results. *Journal of Geophysical Research: Space Physics*, *122*, 547–578. https://doi.org/10.1002/2016JA023167

Hellinger, P., & Mangeney, A. (1997). Upstream whistlers generated by protons reflected from a quasi-perpendicular shock. *Journal of Geophysical Research*, *102*(A5), 9809–9819. https://doi.org/10.1029/96JA03826

Hellinger, P., Mangeney, A., & Matthews, A. (1996). Whistler waves in 3-D hybrid simulations of quasi-perpendicular shocks. *Geophysical Research Letters*, *23*(6), 621–624. https://doi.org/10.1029/96GL00453

Hellinger, P., Traávníček, P., Lembége, B., & Savoini, P. (2007). Emission of nonlinear whistler waves at the front of perpendicular supercritical shocks: Hybrid versus full particle simulations. *Geophysical Research Letters*, *34*, L14109. https://doi.org/10.1029/2007GL030239

Heppner, J. P., Sugiura, M., Skillman, T. L., Ledley, B. G., & Campbell, M. (1967). OGO—A magnetic field observations. *Journal of Geophysical Research*, *72*(21), 5417–5471. https://doi.org/10.1029/JZ072i021p05417

Holzer, R. E., Northrop, T. G., Olson, J. V., & Russell, C. T. (1972). Study of waves in the Earth's bow shock. *Journal of Geophysical Research*, *77*(13), 2264–2273. https://doi.org/10.1029/JA077i013p02264

Hoppe, M. M., & Russell, C. T. (1980). Whistler mode wave packets in the Earth's foreshock region. *Nature*, *287*, 417–420. https://doi.org/10.1038/287417a0

Hoppe, M. M., Russell, C. T., Eastman, T. E., & Frank, L. A. (1982). Characteristics of the ULF waves associated with upstream ion beams. *Journal of Geophysical Research*, *87*(A2), 643–650. https://doi.org/10.1029/JA087iA02p00643

Hoppe, M. M., Russell, C. T., Frank, L. A., Eastman, T. E., & Greenstadt, E. W. (1981). Upstream hydromagnetic waves and their association with backstreaming ion populations: ISEE 1 and 2 observations. *Journal of Geophysical Research*, *86*(A6), 4471–4492. https://doi.org/10.1029/JA086iA06p04471

Jakosky, B. M., Lin, R. P., Grebowsky, J. M, Luhmann, J. G, Mitchell, D. F, Beutelschies, G., et al. (2015). The Mars Atmosphere and Volatile EvolutioN (MAVEN) mission. *Space Science Reviews*, *195*(1–4), 3–48. https://doi.org/10.1007/s11214-015-0139-x

Krasnoselskikh, V. V., Lembége, B., Savoini, P., & Lobzin, V. V. (2002). Nonstationarity of strong collisionless quasiperpendicular shocks: Theory and full particle numerical simulations. *Physics of Plasmas*, *9*, 1192–1209. https://doi.org/10.1063/1.1457465

Krauss-Varban, D., Pantellini, F. G. E., & Burgess, D. (1995). Electron dynamics and whistler waves at quasi-perpendicular shocks. *Geophysical Research Letters*, *22*(16), 2091–2094. https://doi.org/10.1029/95GL01782

Lacombe., C., Alexandrova, O., Matteini, L., Santolík, O., Cornilleau-Wehrlin, N., Mangeney, A., et al. (2014). Whistler mode waves and the electron heat flux in the solar wind: Cluster observations. *The Astrophysical Journal*, *796*, 5. https://doi.org/10.1088/0004-637X/796/1/5

Le, G., Chi, P. J., Blanco-Cano, X., Boardsen, S., Slavin, J. A., & Anderson, B. J. (2013). Upstream ultra-low frequency waves in Mercury's foreshock region: MESSENGER magnetic field observations. *Journal of Geophysical Research: Space Physics*, *118*, 2809–2823. https://doi.org/10.1002/jgra.50342

Leroy, M. M., Winske, D., Goodrich, C. C., Wu, C. S., & Papadopoulos, K. (1982). The structure of perpendicular bow shocks. *Journal of Geophysical Research*, *87*(A7), 5081–5094. https://doi.org/10.1029/JA087iA07p05081

Mazelle, C., Winterhalter, D., Sauer, K, Trotignon, J. G., Acuña, M. H., Baumgärtel, K., et al. (2004). Bow shock and upstream phenomena at Mars. *Space Science Reviews*, *111*, 115–181. https://doi.org/10.1023/B: SPAC.0000032717.98679.d0

Meziane, K., Mazelle, C. X., Romanelli, N., Mitchell, D. L., Espley, J. R., Connerney, J. E. P., et al. (2017). Martian electron foreshock from MAVEN observations. *Journal of Geophysical Research: Space Physics*, *122*, 1531–1541. https://doi.org/10.1002/2016JA023282

Nakagawa, T., Takahashi, F., Tsunakawa, H., Shibuya, H., Shimizu, H., & Matsushima, M. (2011). Non-monochromatic whistler waves detected by Kaguya on the dayside surface of the Moon. *Earth Planets Space*, *63*(1), 37–46. https://doi.org/10.5047/eps.2010.01.005

Nakagawa, T., Takahashi, Y., & Iizima, M. (2003). GEOTAIL observation of upstream ULF waves associated with lunar wake. *Earth, Planets and Space*, *55*, 569–580. https://doi.org/10.1186/BF03351789

Orlowski, D. S., Crawford, G. K., & Russell, C. T. (1990). Upstream waves at Mercury, Venus and Earth: Comparison of the properties of one hertz waves. *Geophysical Research Letters*, *17*(13), 2293–2296. https://doi.org/10.1029/GL017i013p02293

Orlowski, D. S., & Russell, C. T. (1991). Ulf waves upstream of the Venus bow shock: Properties of one-hertz waves. *Journal of Geophysical Research*, *96*(A7), 11,271–11,282. https://doi.org/10.1029/91JA01103

Orlowski, D. S., Russell, C. T., Krauss-Varban, D., Omidi, N., & Thomsen, M. F. (1995). Damping and spectral formation of upstream whistlers. *Journal of Geophysical Research*, *100*(A9), 17,117–17,128. https://doi.org/10.1029/95JA00062

Orlowski, D. S., Russell, C. T., & Lepping, R. P. (1992). Wave phenomena in the upstream region of Saturn. *Journal of Geophysical Research*, *97*(A12), 19,187–19,199. https://doi.org/10.1029/92JA01461

Ramírez Vélez, J. C., Blanco-Cano, X., Aguilar-Rodriguez, E., Russell, C. T., Kajdič, P., Jian, L. K., & Luhmann, J. G. (2012). Whistler waves associated with weak interplanetary shocks. *Journal of Geophysical Research*, *117*, A11103. https://doi.org/10.1029/2012JA017573

Romanelli, N., Mazelle, C., Chaufray, J. Y., Meziane, K., Shan, L., Ruhunusiri, S., et al. (2016). Proton cyclotron waves occurrence rate upstream from Mars observed by MAVEN: Associated variability of the Martian upper atmosphere. *Journal of Geophysical Research: Space Physics*, *121*, 11,113–11,128. https://doi.org/10.1002/2016JA023270

Romanelli, N., Bertucci, C., Gmez, D., Mazelle, C., & Delva, M. (2013). Proton cyclotron waves upstream from Mars: Observations from Mars Global Surveyor. *Planetary and Space Science*, *76*, 1–9.

Ruhunusiri, S., Halekas, J. S., Connerney, J. E. P., Espley, J. R., McFadden, J. P., Mazelle, C., et al. (2016). MAVEN observation of an obliquely propagating low-frequency wave upstream of Mars. *Journal of Geophysical Research: Space Physics*, *121*, 2374–2389. https://doi.org/10.1002/2015JA022306

Ruhunusiri, S., Halekas, J. S., Espley, J. R., Mazelle, C., Brain, D., Harada, Y., et al. (2017). Characterization of turbulence in the Mars plasma environment with MAVEN observations. *Journal of Geophysical Research: Space Physics*, *122*, 656–674. https://doi.org/10.1002/2016JA023456

Russell, C. T. (2007). Upstream whistler-mode waves at planetary bow shocks: A brief review. *Journal of Atmospheric and Terrestrial Physics*, *69*, 1739–1746. https://doi.org/10.1016/j.jastp.2006.11.004

Russell, C. T., Childers, D. D., & Coleman, P. J., Jr. (1971). Ogo 5 observations of upstream waves in the interplanetary medium: Discrete wave packets. *Journal of Geophysical Research*, *76*(4), 845–861. https://doi.org/10.1029/JA076i004p00845

Russell, C. T., & Farris, M. H. (1995). Ultra low frequency waves at the Earth's bow shock. *Advances in Space Research*, *15*, 285–296.

Russell, C. T., Luhmann, J. G., Schwingenschuh, K., Riedler, W., & Yeroshenko, Y. e. (1990). Upstrem waves at Mars: Phobos observations. *Geophysical Research Letters*, *17*, 897–900.

Sentman, D. D., Thomsen, M. F., Gary, S. P., Feldman, W. C., & Hoppe, M. M. (1983). The oblique whistler instability in the Earth's foreshock. *Journal of Geophysical Research*, *88*(A3), 2048–2056. https://doi.org/10.1029/JA088iA03p02048

Smith, C. W., Goldstein, M. L., & Wong, H. K. (1989). Whistler wave bursts upstream of the Uranian bow shock. *Journal of Geophysical Research*, *94*(A12), 17,035–17,048. https://doi.org/10.1029/JA094iA12p17035

Smith, C. W., Wong, H. K., & Goldstein, M. L. (1991). Whistler waves associated with the Uranian bow shock: Outbound observations. *Journal of Geophysical Research*, *96*(A9), 15,841–15,852. https://doi.org/10.1029/91JA01460

Sulaiman, A. H., Gurnett, D. A., Halekas, J. S., Yates, J. N., Kurth, W. S., & Dougherty, M. K. (2017). Whistler mode waves upstream of Saturn. *Journal of Geophysical Research: Space Physics*, *122*, 227–234. https://doi.org/10.1002/2016JA023501

Tsurutani, B. T., Glassmeier, K.-H., & Neubauer, F. M. (1995). An intercomparison of plasma turbulence at three comets: Grigg-Skjellerup, Giacobini-Zinner, and Halley. *Journal of Geophysical Research*, *22*, 1149–1152. https://doi.org/10.1029/95GL00806

Tsurutani, B. T., Smith, E. J., Burton, M. E., Arballo, J. K., Galvan, C., Zhou, X.-Y., et al. (2001). Oblique 1-Hz whistler mode waves in an electron foreshock: The Cassini near-Earth encounter. *Journal of Geophysical Research*, *106*(A12), 30,223–30,238. https://doi.org/10.1029/2001JA900108

Tsurutani, B. T., Southwood, D. J., Smith, E. J., & Balogh, A. (1993). A survey of low frequency waves at Jupiter: The Ulysses encounter. *Journal of Geophysical Research*, *98*(A12), 21,203–21,216. https://doi.org/10.1029/93JA02586

Tsugawa, Y., Katoh, Y., Terada, N., Ono, T., Tsunakawa, H., Takahashi, F., et al. (2012). Statistical study of broadband whistler-mode waves detected by Kaguya near the Moon. *Geophysical Research Letters*, *39*, L16101. https://doi.org/10.1029/2012GL052818

Tsugawa, Y., Katoh, Y., Terada, N., Ono, T., Tsunakawa, H., Takahashi, F., et al. (2014). Group-standing of whistler mode waves near the Moon. *Journal of Geophysical Research: Space Physics*, *119*, 2634–2648. https://doi.org/10.1002/2013JA019585

Tsugawa, Y., Katoh, Y., Terada, N., Ono, T., Tsunakawa, H., Takahashi, F., et al. (2015). Harmonics of whistler-mode waves near the Moon. *Earth, Planets, and Space*, *67*, 36. https://doi.org/10.1186/s40623-015-0203-5

Tsugawa, Y., Terada, N., Katoh, Y., Ono, T., Tsunakawa, H., Takahashi, F., et al. (2011). Statistical analysis of monochromatic whistler waves near the Moon detected by Kaguya. *Annales de Geophysique*, *29*, 889–893.

Walker, S. N., Balikhin, M. A., & Nozdrachev, M. N. (1999). Ramp nonstationarity and the generation of whistler waves upstream of a strong quasiperpendicular shock. *Geophysical Research Letters*, *26*(10), 1357.

Wilson, L. B., Cattell, C. A., Kellogg, P. J., Goetz, K., Kersten, K., Kasper, J. C., et al. (2009). Low-frequency whistler waves and shocklets observed at quasi-perpendicular interplanetary shocks. *Journal of Geophysical Research*, *114*, A10106. https://doi.org/10.1029/2009JA014376

Wong, H. K., & Goldstein, M. L. (1987). Proton beam generation of whistler waves in the Earth's foreshock. *Journal of Geophysical Research*, *92*(A11), 12,419–12,424. https://doi.org/10.1029/JA092iA11p12419

Wong, H. K., & Goldstein, M. L. (1988). Proton beam generation of oblique whistler waves. *Journal of Geophysical Research*, *93*(A5), 4110–4114. https://doi.org/10.1029/JA093iA05p04110

Wong, H. K., & Smith, C. W. (1994). Electron beam excitation of upstream waves in the whistler mode frequency range. *Journal of Geophysical Research*, *99*(A7), 13,373–13,387. https://doi.org/10.1029/94JA00821

Yamauchi, M., Hara, T., Lundin, R., Dubinin, E., Fedorov, A., Sauvaud, J.-A., et al. (2015). Seasonal variation of Martian pick-up ions: Evidence of breathing exosphere. *Planetary and Space Science*, *119*, 54–61. https://doi.org/10.1016/j.pss.2015.09.013

Yamauchi, M., Futaana, Y., Fedorov, A., Frahm, R. A., Winningham, J. D., Dubinin, E., et al. (2011). Comparison of accelerated ion populations observed upstream of the bow shocks at Venus and Mars. *Annales de Geophysique*, *29*, 511–528.